Available online www.jocpr.com

Journal of Chemical and Pharmaceutical Research, 2016, 8(5):420-438

Research Article

ISSN : 0975-7384
CODEN(USA) : JCPRC5

Optimal design of magnetic field for reaction control in drug delivery applications

A. J. Keikha[1] and M. Y. Abdollahzadeh[1,2]

[1]Chabahar Maritime University, Chabahar, Iran
[2]Department of Mechanical, Robotics and Energy Engineering, Dongguk University-Seoul, 30 Pildong-ro 1gil, Jung-gu, Seoul 100-715, Republic of Korea

---

ABSTRACT

We present an optimal design of magnetic field for reaction control in drug delivery applications by nonlinear topology optimization method. In this model, the objective is to find the optimal distribution of a magnetic field in a blood artery such that the axial velocity component at the center of the channel is minimized. Our implementation allows a wide range of optimization objectives, such as gene transfer and drug delivery, to be dealt with straightforwardly. Topology optimization of the Navier-Stokes equations is encountered in different branches and applications. We demonstrate our method by studies of steady-state Navier–Stokes flow problems, as well as encompassing the topology optimization of fluids in Stokes flow. We analyze the physical aspects of the solutions and how they are affected by different parameters of the optimization algorithm.

Keywords: topology optimization, reactive fluid flow, Navier–Stokes flow, inertial effects, drug delivery

---

INTRODUCTION

In recent decades, progression of nano-technology [1-4], many theoretical phenomena have originated their reputation in emerging applications [5-10]. Targeted drug delivery by using magnetic nanoparticles is an efficient technique to deliver drug molecules to specific tissues in an animal [11-15]. An electromagnetic actuation system is a promising solution for applying an adequate force to direct the magnetic nanoparticles in the blood vessels in a noninvasive way [16-25]. To do that a combined actuation and monitoring system is required to provide a closed-loop nanoparticle localization of the magnetic nanoparticles on the basis of magnetic particle imaging for more precise targeting [26-30]. The magnetic nanoparticles can be navigated by applying a magnetic field gradient provided by the actuation system and monitored by applying the drive and selection fields to the actuation coils by using a time division multiplexing scheme [31-35]. Between various nanoparticle types, the silver nanoparticles (AgNps) are extensively investigated because of wide range applications such as antibacterial, catalyst, medical devices, photonics, optoelectronics and biosensors [36-37]. Usually metallic nanoparticles are synthesized by chemical, mechanical and electrochemical methods [38]. In these methods for the synthesis of silver nanoparticles used toxic chemicals compounds that can have negative effects on the environment and water ecosystems.

The magnetic field distribution method in topology optimization was originally developed for stiffness design of mechanical structures [2] but has now been extended to a multitude of design problems in structural mechanics as well as to optics and acoustics [3, 4, 5, 6]. Recently Borrvall and Petersson introduced the method for fluids in Stokes flow [1]. However, it is desirable to extend the method to fluids described in a full Navier–Stokes flow; a direction pioneered by the work of Sigmund and Gersborg-Hansen [7, 8, 9]. It has a wider range of applicability than the Navier–Stokes problems studied here, and moreover it allows a wide range of optimization objectives to be dealt with easily. Extending the topology optimization method to new physical domains generally involves some rethinking of the design problem and some" trial and error" to determine suitable design objectives. It also requires

the numerical analysis and implementation of the problem, e.g., using the finite element method (FEM). This process is accelerated a lot by using a high-level FEM library or package that allows different physical models to be joined and eases the tasks of geometry setup, mesh generation, and post processing. The disadvantage is that high-level packages tend to have rather complex data structure, not easily accessible to the user. This can complicate the actual implementation of the problem because the sensitivity analysis is traditionally formulated in a low-level manner. We show how this sensitivity analysis can be performed in a simple way that is almost independent of the particular physical problem studied. This approach proves even more useful for multi-field extensions, where the flow problem is coupled to, e.g., heat conduction, convection-diffusion of solutes, and deformation of elastic channel walls in valves and flow rectifiers [10]. The paper is organized as follows: In Sec. II we introduce the topology optimization method for fluids in Navier– Stokes flow, and discuss the objective of designing fluidic devices or channel networks for which the power dissipation is minimized [11, 12, 13].

To investigate the feasibility of combining the actuation system an MPI system is required which used an efficient numerical simulations and optimizing hardware constraints. The challenge of that aim is to sequence the actuation signal and the MPI signal to perform both tasks simultaneously. The simulation results showed the feasibility of the MPI-based actuation system. The proposed system will provide simultaneous navigation and tracking for targeted drug delivery of MNPs in compact and efficient ways. As a result of the devastating effects of these methods on the marine environment, at present several methods for the synthesis of these nanomagnetic fields are necessary. One of these methods that's more compatible with the environment and create less pollution, are biological methods. In this method to synthesis metal nanoparticles, used microorganism and plant magnetic fields that exist in nature instead of toxic chemicals [39]. One of the resources that can be used in nanotechnology and synthesis of nanoparticles are seaweeds that have variety types of phytochemical compounds such as proteins, carbohydrates, alkaloids, steroids, phenols, saponins and flavonoids [40] play key role in bio reduction of the metal ions into Nano form. Toxicity of silver ion has been known for centuries but silver nanoparticles toxicity may be dependent on particle concentration, particle size and shape and surface chemistry [41]. In recent years, several studies have been conducted regarding to the effect of silver nanoparticles synthesized by chemical methods on fish toxicity [42-45].

Although our high-level programming-language implementation is generally applicable we have chosen to start on the concrete level by treating the basic equations for our main example: the full steady-state Navier–Stokes flow problem for incompressible fluids. We consider a given computational domain with appropriate boundary conditions for the flow given on the domain boundary. The goal of the optimization is to distribute a certain amount of solid magnetic field inside such that the magnetic field layout defines a fluidic device or channel network that is optimal with respect to some objective, formulated as a function of the variables, e.g., minimization of the power dissipated inside the domain. The basic principle in the magnetic field distribution method for topology optimization is to replace the original discrete design problem with a continuous one where the magnetic field density is allowed to vary continuously between solid and void [3]. Thus in our flow problem we assume the design domain to be filled with some idealized magnetic field of spatially varying magnetic field strength. Solid wall and open channels then correspond to the limits of very low and very high magnetic field strength, respectively. In the final design there should preferably be no regions at intermediate magnetic field strength since otherwise it cannot be interpreted as a solution to the original discrete problem. Alternatively it may be possible to fabricate the device from polymeric magnetic fields such as PDMS that naturally have a finite magnetic field strength to the fluid [14]. Through the literature search [46-63], no researches have studied the applicability of using Ag nanoparticles for drug delivery in animals. Magnetic drug targeting is a drug delivery approach in which therapeutic magnetizable particles are injected, generally into blood vessels, and magnets are then used to guide and concentrate them in the diseased target organ. Previous study [63] done by author and cooperators is the first study on the toxicity of silver nanoparticles synthesized using biological methods on common carp. The purpose of this study is feasibility study of magnetic effects on silver nanoparticles for drug and gene delivery in fishes. The present invention provides a two-dimensional analysis using differential equations of fluid flow for the purpose of delivering magnetic nanoparticles

EXPERIMENTAL SECTION

The applicability of the current study requires a drive device which is adapted such that particle magnetization and electromagnetic field gradient can be simultaneously satisfied by using a DCC system, and is adapted such that the overall three-dimensional drive unit size can be minimized by reducing the number of coils and current-supply units, and is able to generate a high electromagnetic field gradient and a high particle drive force by inserting cores in the centers of the coils and thereby concentrating the electromagnetic field. Figure 1 depicts the schematic of the flux density distribution on a blood artery. The coil is in the X-Y plane and Magnetic Field is evaluated. The flow is 2-dimensioanl, laminar and non-Newtonian. We assume that the fluid flowing in the idealized medium is subject to a friction force f which is proportional to the fluid velocity v. Thus $f = -\alpha v$, where $\alpha(r)$ is the inverse of the local

magnetic field of the medium at position r. These properties of the idealized medium may only be approximately valid for an actual medium. However, the assumptions are not in conflict with any fundamental physical law, and since the converged solutions contain only solid walls and open channels, the specific nature of the idealized medium is of no consequence. The flow problem is described in terms of the fluid velocity field v(r) where $\vec{v}=(v_1(\vec{r}),v_2(\vec{r}))$ and pressure p(r)where $\vec{r}=(x_1,x_2)$. The governing equations are the steady state Navier–Stokes equation and the incompressibility constraint

$$\rho(\vec{v}.\nabla)\vec{v}=\nabla.\sigma-\alpha\vec{v} \tag{1}$$

$$\nabla.\vec{v}=0 \tag{2}$$

where ρ is the mass density of the fluid. For an incompressible Newtonian fluid the components σ_{ij} of the Cauchy stress tensor σ are given by

$$\sigma_{ij}=-p\delta_{ij}+\eta\left(\frac{\partial v_i}{\partial x_j}+\frac{\partial v_j}{\partial x_i}\right) \tag{3}$$

It is convenient to introduce a design variable field γ(r) controlling the local magnetic field strength of the medium. We let γ vary between zero and unity, with γ = 0 corresponding to magnetic magnetic field and γ = 1 to no magnetic magnetic field. Following Ref. [1] we then relate the local inverse magnetic field strength α(r) to the design field γ(r) by the convex interpolation

$$\alpha(\gamma)\equiv\alpha_{\min}+(\alpha_{\max}-\alpha_{\min})\frac{q[1-\gamma]}{q+\gamma} \tag{4}$$

where q is a real and positive parameter used to tune the shape of α(γ). Ideally, impermeable solid walls would be obtained with $\alpha_{max}=\infty$, but for numerical reasons we need to choose a finite value for α_{max}. For the minimal value we choose α_{min} = 0.[19] For a given magnetic field distribution γ(r) there are two dimensionless numbers characterizing the flow, namely the Reynolds number

$$\mathrm{Re}=\frac{\rho l v}{\eta} \tag{5}$$

Hartmann number (Ha) is the ratio of electromagnetic force to the viscous force first introduced by Hartmann.[1] It is defined by:

$$Ha=\rho l\sqrt{\frac{\sigma}{\eta}} \tag{6}$$

B is the magnetic field, L is the characteristic length scale, σ is the electrical conductivity, μ is the dynamic viscosity. In the pioneering work by Borrvall and Petersson [1] the main focus was on minimizing the power dissipation in the fluid. The total power dissipated inside the fluidic system (per unit length in the third dimension) is given by [15]

$$\Phi(\mathbf{v},p,\gamma)=\int_{\Omega}\left[\frac{1}{2}\eta\sum_{i,j}\left(\frac{\partial v_i}{\partial x_j}+\frac{\partial v_j}{\partial x_i}\right)^2+\sum_i\alpha(\gamma)v_i^2\right]dr \tag{7}$$

In steady-state this is equal to the sum of the work done on the system by the external forces and the kinetic energy converted into it,

$$\Phi(\mathbf{v},p,\gamma)=\int_{\partial\Omega}\sum_{i,j}\left[n_i\sigma_{ij}v_j-n_iv_i(\frac{1}{2}\rho v_j^2)\right]ds \tag{8}$$

Here n is a unit outward normal vector such that n· σ is the external force acting on the system boundary and n· σ ·v is the work done on the system by this force. Moreover, in the common case where the geometry and boundary conditions are such that the no-slip condition v = 0 applies on all external solid walls, while on the inlet and outlet boundaries v is parallel to n and (n ·∇) v = 0, [20] Eq. (7) reduces to

$$\Phi(\mathbf{v}, p, \gamma) = \int_{\partial\Omega} -\mathbf{n}.\mathbf{v}(p + \frac{1}{2}\rho v^2)ds \quad (9)$$

Borrvall and Petersson showed that for Stokes flow with Dirichlet boundary conditions everywhere on the boundary ∂Ω, the *problem of minimizing the total power dissipation inside the fluidic device subject to a volume constraint on the magnetic field distribution* is mathematically well-posed. Moreover it was proven that in the case where α(γ) is a linear function, the optimal magnetic field distribution is fully discrete-valued. When α(γ) is not linear but convex then the solid/void interfaces in the optimal solution are not discrete zero/unity transitions but slightly smeared out. Convexity implies that the (negative value of the) slope of α at γ = 0 is larger than at γ = 1; therefore there will be a neighborhood around the discrete interface where it pays to move magnetic field from the solid side to the void. Using the interpolation in Eq. (4) we have

$$\alpha'(0) = (\alpha_{min} - \alpha_{max})(1+q)/q \quad (10)$$

and

$$\alpha'(1) = (\alpha_{min} - \alpha_{max})\, q/\, 1+q \quad (11)$$

For large values of q the interpolation is almost linear and we expect almost discrete interfaces, whereas for small q we expect smeared out interfaces in the optimized solution. Consider the case when Eq. (8) applies. If the system is driven with a prescribed flow rate then minimizing the total power dissipation is clearly equivalent to minimizing the pressure drop across the system. Conversely, if the system is driven at a prescribed pressure drop, then the natural design objective will be to maximize the flow rate which is equivalent to maximizing the dissipated power, c.f. Eq. (9).

In either case the objective can be described as minimizing the hydraulic resistance of the system. For problems with more complex design objectives, such as a minimax problem for the flow rate through several different outlets, there will typically be no analog in terms of total dissipated power. In such cases there is no guarantee for the existence of a unique optimal solution and one has to be extra careful when formulating the design problem.

A permanent magnet is placed over the top wall of the channel. The center of this permanent magnet is located at 3mm from the top wall of the vessel, see Figure 1. The external permanent magnetic field is applied vertically with it intensity at the center equal to 10^6 A/m and its diameter equal to 4mm, as shown by Figure 1. Here we deal with the design of a structure that at a particular point inside a long straight channel can guide the flow in the opposite direction of the applied pressure drop. The corresponding problem with a prescribed flow rate was first suggested and investigated by A. Gersborg-Hansen [8]. We elaborate on it here to illustrate the importance of the choice of magnetic field strength for the medium. The computational domain is shown in Fig. 1. It consists of a long straight channel of height ℓ and length L = 10ℓ; the actual design domain, inside which the magnetic field is distributed, is limited to the central part of length 5ℓ. The boundary conditions prescribe a pressure drop of p from the inlet (left) to the outlet (right), and no-slip for the fluid on the channel side walls.

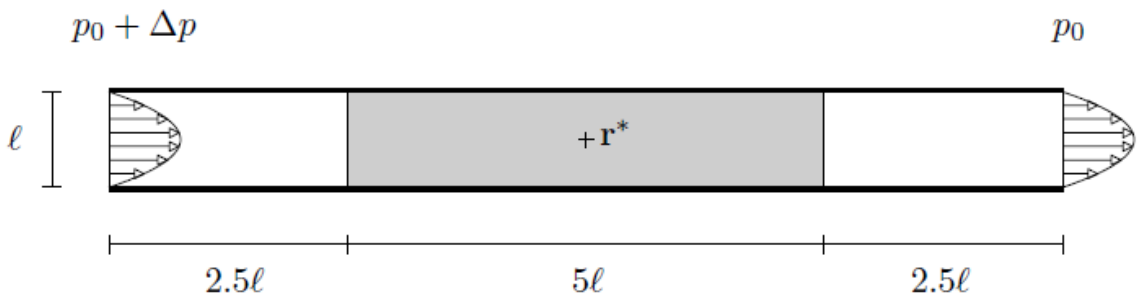

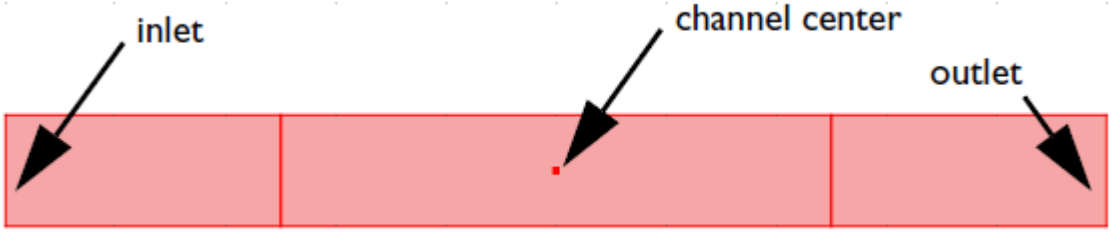

Fig.1. Computational domain for the reverse flow example. The design domain (gray) has length 5ℓ and height ℓ, and the fluid enters and leaves the design domain through leads of length 2.5ℓ. The boundary conditions prescribe a pressure drop of p across the system, and the design objective is to reverse the flow direction at the center of the channel

RESULTS AND DISCUSSION

Using this, Eqs. (1) and (2) can be written in divergence form as

$$\nabla.\Gamma_i = F_i \quad \text{in} \quad \Omega \tag{12}$$

$$R_i = 0 \quad \text{on} \quad \partial\Omega \tag{13}$$

$$-\mathbf{n}.\Gamma_i = G_i + \sum_{j=1}^{3} \frac{\partial R_j}{\partial u_i}\mu_j \quad \text{on} \quad \partial\Omega \tag{14}$$

We first introduce the velocity-pressure vector u = [v1, v2, p] and define for i = 1, 2, 3 the quantities as

$$\Gamma_1 \equiv \begin{bmatrix} \sigma_{11} \\ \sigma_{21} \end{bmatrix} \qquad \Gamma_2 \equiv \begin{bmatrix} \sigma_{12} \\ \sigma_{22} \end{bmatrix} \qquad \Gamma_3 \equiv \begin{bmatrix} 0 \\ 0 \end{bmatrix} \tag{15}$$

and

$$F_1 \equiv \rho(\mathbf{v}.\nabla)v_1 + \alpha(\gamma)v_1 \qquad F_2 \equiv \rho(\mathbf{v}.\nabla)v_2 + \alpha(\gamma)v_2 \qquad F_3 \equiv \nabla.\mathbf{v} \tag{16}$$

where Fi are understood to be functions of the solution u, its gradient ∇u, and of the design variable γ. The quantity Ri(u, γ) in Eq. (10) describes Dirichlet type boundary conditions. For example, fluid no-slip boundary conditions are obtained by defining R1 ≡ v1 and R2 ≡ v2 on the external solid walls. The quantity Gi(u, γ) in Eq. (10) describe Neumann type boundary conditions, and μi denote the Lagrange multiplier necessary to enforce the constraint Ri = 0, e.g., the force with which the solid wall has to act upon the fluid to enforce the no-slip boundary condition. Of course, it is not possible to enforce both Dirichlet and Neumann boundary conditions for the same variable simultaneously. Only when the variable u_i is not fixed by any of the Dirichlet constraints Rj does the Neumann condition G_i come into play, as all ∂Rj/∂ui vanish and the Lagrange multipliers μ_j are decoupled from Eq. (10). Inactive Dirichlet constraints can be obtained simply by specifying the zero-function Ri ≡ 0, that also satisfies Eq. (10) trivially.

In general the design objective for the optimization is stated as the minimization of a certain objective function (u, γ). We shall consider a generic integral-type objective function of the form

$$\Phi(\mathbf{u},\gamma) = \int_{\Omega} A(\mathbf{u},\gamma)dr + \int_{\partial\Omega} B(\mathbf{u},\gamma)ds \tag{17}$$

In particular, we can treat the design objective of minimizing the power dissipation inside the fluidic domain by taking,

$$A \equiv \frac{1}{2}\eta\sum_{i,j}\left(\frac{\partial v_i}{\partial x_j} + \frac{\partial v_j}{\partial x_i}\right)^2 + \sum_i \alpha(\gamma)v_i^2 \quad \text{in} \quad \Omega \qquad B \equiv 0 \qquad \text{on} \quad \partial\Omega \tag{18}$$

Alternatively, the objective of maximizing the flow out through a particular boundary segment is obtained by choosing

$$A \equiv 0 \quad \text{in} \quad \Omega \qquad \text{and} \qquad B \equiv \begin{cases} -\mathbf{n}.\mathbf{v} \; on \quad \partial\Omega_0 \\ 0 \quad on \; \partial\Omega / \partial\Omega_0 \end{cases} \tag{19}$$

and objectives related to N discrete points rk can be treated using Dirac delta functions as

$$A \equiv \sum_{k=1}^{N} A_k(\mathbf{u}, \gamma)\delta(r - r_k) \quad \text{in} \quad \Omega \quad \text{and} \quad B \equiv 0 \quad \text{on} \quad \partial\Omega \tag{20}$$

Finally we stress that not all optimization objectives lend themselves to be expressed in the form of Eq. (11) – an example of which is the problem of maximizing the lowest vibrational Eigen frequency in structural mechanics. The optimal design problem can now be stated as a continuous constrained nonlinear optimization problem:

$$\min_{\gamma} \Phi(\mathbf{u}, \gamma) \tag{21}$$

Subject to
Volume constraint

$$\int_{\Omega} \gamma(r)dr - \beta|\Omega| \le 0 \tag{22}$$

Design variable bounds

$$0 \le \gamma(r) \le 1 \tag{23}$$

Governing equations

$$\nabla.\Gamma_i = F_i \quad \text{in} \quad \Omega \tag{24}$$

$$R_i = 0 \quad \text{on} \quad \partial\Omega \tag{25}$$

$$-\mathbf{n}.\Gamma_i = G_i + \sum_{j=1}^{3} \frac{\partial R_j}{\partial u_i}\mu_j \quad \text{on} \quad \partial\Omega \tag{26}$$

With the volume constraint we require that at least a fraction 1 − β of the total volume should be filled with magnetic field. The very reason for replacing the original discrete design problem with a continuous one by assuming a magnetic field is that it allows the use of efficient mathematical programming methods for smooth problems. We have chosen the popular method of moving asymptotes (MMA) [11, 12], which is designed for problems with a large number of degrees-of-freedom and thus well-suited for topology optimization [3]. It is a gradient-based algorithm requiring information about the derivative with respect to γ of both the objective function and the constraints. Notice that for any γ the governing equations allow us to solve for u; therefore in effect they define u[γ] as an implicit function. The gradient of objective function is then obtained using the chain rule

$$\frac{d}{d\gamma}\left[\Phi(\mathbf{u}[\gamma], \gamma)\right] = \frac{\partial\Phi}{\partial\gamma} + \int_{\Omega} \frac{\partial\Phi}{\partial\mathbf{u}}.\frac{\partial\mathbf{u}}{\partial\gamma}dr \tag{27}$$

However, because u[γ] is implicit, it is impractical to evaluate the derivative ∂u/∂γ directly. Instead, we use the ad joint method to eliminate it from Eq. (16) by computing a set of Lagrange multipliers for Eqs. (8) to (11) considered as constraints [16].

The optimization process is iterative and the kth iteration consists of three steps:
(i) Given a guess γ(k) for the optimal magnetic field distribution we first solve Eqs. (10) to (12) for u(k) as a finite element problem
(ii) Next, the sensitivity analysis is performed where the gradient of the objective and constraints with respect to γ is evaluated. In order to eliminate ∂u/∂γ from Eq. (16) we solve the adjoint problem of Eqs. (10) to (12) for the Lagrange multipliers eu(k).
(iii) Finally, we use MMA to obtain a new guess γ(k+1) for the optimal design based on the gradient information and the past iteration history.

Of the three steps, (i) is the most expensive computational wise since it involves the solution of a nonlinear partial differential equation.
The starting point of the finite element analysis is to approximate the solution component ui on a set of finite element basis functions,

$$u_i(\mathbf{r}) = \sum_n u_{i,n}\varphi_{i,n}(\mathbf{r}) \tag{28}$$

where ui,n are the expansion coefficients. Similarly, the design variable field γ(r) is expressed as

$$\gamma(\mathbf{r}) = \sum_n \gamma_n \varphi_{4,n}(\mathbf{r}) \tag{29}$$

For our incompressible Navier–Stokes problem we use the standard Taylor–Hood element pair with quadratic velocity approximation and linear pressure. For the design variable we have chosen the linear Lagrange element.[21] The problem Eqs. (10) to (13) is discretized by the Galerkin method and takes the form

$$\mathbf{L}_i(\mathbf{U},\gamma) - \sum_{j=1}^{3} \mathbf{N}_{ji}^T \Lambda_j = 0 \qquad \text{and} \qquad \mathbf{M}_i(\mathbf{U},\gamma) = 0 \tag{30}$$

where Ui are column vectors holding the expansion coefficients for the solution ui,n, the Lagrange multipliers μi,n, and the design variable field γn, respectively. The column vector Li contains the projection of Eq. (10a) onto ϕi,n which upon partial integration is given by

$$\mathbf{L}_{i,n} = \int_\Omega (\varphi_{i,n} F_i + \nabla\varphi_{i,n}.\Gamma_i)dr + \int_{\partial\Omega} \varphi_{i,n} G_i ds \tag{31}$$

The column vector Mi contains the point wise enforcement of the Dirichlet constraint

$$\mathbf{M}_{i,n} = R_i(\mathbf{u}(r_{i,n})) \tag{32}$$

Finally, the matrix
$N_{ij} = -\partial M_i/\partial U_j$ (33)

describes the coupling to the Lagrange multipliers in Eq. (10). The solution of the nonlinear system in Eq. (19) above corresponds to step (i) in kth iteration. The sensitivity analysis in step (ii) requires us to compute

$$\frac{d}{d\gamma}[\Phi(\mathbf{U}[\gamma],\gamma)] = \frac{\partial\Phi}{\partial\gamma} + \sum_{i=1}^{3} \frac{\partial\Phi}{\partial\mathbf{U}_i}\frac{\partial\mathbf{U}_i}{\partial\gamma} \tag{34}$$

which is done using the standard adjoint method [16]. By construction we have for any that

$$\mathbf{L}_i(\mathbf{U}(\gamma),\gamma) - \sum_{j=1}^{3} \mathbf{N}_{ji}^T \Lambda_j(\gamma) = 0 \tag{35}$$

and

$$\mathbf{M}_i(\mathbf{U}(\gamma),\gamma) = 0 \tag{36}$$

Therefore also the derivative of those quantities with respect to is zero, and adding any multiple to Eq. (22a) does not change the result

$$\frac{d}{d\gamma}[\Phi(\mathbf{U}[\gamma],\gamma)] = \frac{\partial\Phi}{\partial\gamma} + \sum_{i=1}^{3}\frac{\partial\Phi}{\partial\mathbf{U}_i}\frac{\partial\mathbf{U}_i}{\partial\gamma} + \sum_{i=1}^{3}\left[\tilde{\mathbf{U}}_i^T \frac{\partial}{\partial\gamma}\left(\mathbf{L}_i - \sum_{j=1}^{3}\mathbf{N}_{ji}^T\Lambda_j\right) - \tilde{\Lambda}_i^T\frac{\partial}{\partial\gamma}(\mathbf{M}_i)\right]$$
$$= \frac{\partial\Phi}{\partial\gamma} + \sum_{i=1}^{3}\left(\tilde{\mathbf{U}}_i^T\frac{\partial\mathbf{L}_i}{\partial\gamma} - \tilde{\Lambda}_i^T\frac{\partial\mathbf{M}_i}{\partial\gamma}\right) \tag{37}$$

Here we see that the derivatives ∂Uiof the implicit functions can be eliminated by

$$\sum_{j=1}^{3} \mathbf{K}_{ji}^{T} \tilde{\mathbf{U}}_{j} - \mathbf{N}_{ij}^{T} \tilde{\Lambda}_{j} = \frac{\partial \Phi}{\partial \mathbf{U}_{i}} \tag{38}$$

and

$$\sum_{j=1}^{3} \mathbf{N}_{ij}^{T} \tilde{\mathbf{U}}_{j} = 0 \tag{39}$$

where we introduced

$$\mathrm{Kij} = -\partial \mathrm{Li}/\partial \mathrm{Uj} \tag{40}$$

This problem is the adjoint of Eq. (19). In deriving Eq. (22b) we implicitly assumed that Nij is independent of , i.e., that the constraint Ri(u, γ) is a linear function. If this is not true then the gradient ∂/∂ computed from Eq. (22b) is not exact, which may lead to poor performance of the optimization algorithm if the constraints are strongly nonlinear. In order to avoid such problems it is necessary to include the nonlinear parts of the constraint vector M into L and move the corresponding Lagrange multipliers to U.

We end this section by discussing a few issues on the implementation of topology optimization. Firstly there is the question of how to represent the design variable γ(r). The governing equations as expressed by Fi in Eq. (13) depend not only on the solution u but also on γ, and the implementation should allow for this dependence in an efficient way. Here our simple and straightforward approach is to include γ as an extra dependent variable on equal footing with the velocity field and pressure, i.e., we append it to the velocity-pressure vector, redefining u as

$$\mathrm{u} \equiv [\mathrm{v1}, \mathrm{v2}, \mathrm{p}, \gamma]. \tag{41}$$

This was already anticipated when we denoted the basis set for γ by {φ4,n(r)}. By making γ available as a field variable we can take full advantage of all the symbolic differentiation, matrix, and post processing tools for analyzing and displaying the magnetic field distribution. Appending γ to the list of dependent variables we are required to define a fourth governing equation. However, since we are never actually going to solve this equation, but rather update γ based on the MMA step, we simply define

$$\Gamma_4 \equiv \begin{bmatrix} 0 \\ 0 \end{bmatrix} \qquad F_4 \equiv 0 \; G_4 \equiv 0 \; R_4 \equiv 0 \tag{42}$$

It is crucial then that the finite element solver allows different parts of the problem to be solved in a decoupled manner, i.e., it must be possible to solve Eqs. (10)-(13) for ui for i = 1, 2, 3 while keeping u4, i.e., γ, fixed. In the nonlinear problem Eq. (19) is solved using damped Newton iterations [17]. Therefore the matrices Kij = −∂Li/∂Uj and Nij = −∂Mi/∂Uj appearing in the adjoint problem Eq. (23) are computed automatically as part of the solution process and can be obtained directly as Matlab sparse matrices. Kij,

$$\mathbf{K}_{ij,nm} = -\int_{\Omega} \left(\varphi_{i,n} \left[\frac{\partial F_i}{\partial \nabla u_j} . \nabla \varphi_{j,m} \right] + \nabla \varphi_{i,n} . \left[\frac{\partial \Gamma_i}{\partial u_j} \varphi_{ij,m} + \frac{\partial \Gamma_i}{\partial \nabla u_j} . \nabla \varphi_{j,m} \right] \right) dr - \int_{\partial \Omega} \varphi_{i,n} \frac{\partial G_i}{\partial u_j} \varphi_{j,m} ds \tag{43}$$

andNij

$$\mathbf{N}_{ij,nm} = -\frac{\partial \mathbf{R}_i}{\partial u_j}\bigg|_{\mathbf{r}_{i,n}} \varphi_{j,m}(\mathbf{r}_{i,n}) \tag{44}$$

Regarding the right-hand side vector ∂/∂Ui in Eq. (23), notice that for a general objective as Eq. (11), it has the form

$$\frac{\partial \Phi}{\partial u_{i,n}} = \int_{\Omega} \left(\frac{\partial A}{\partial u_i} + \frac{\partial A}{\partial \nabla u_i} . \nabla \right) \varphi_{i,n} d\mathbf{r} + \int_{\partial \Omega} \frac{\partial B}{\partial u_i} \varphi_{i,n} ds \tag{45}$$

It is not in the spirit of a high-level finite element package to program the assembly of this vector by hand. Instead we employ the built-in assembly subroutine of . We construct a copy of the original problem sharing the geometry,

finite element mesh, and degree-of-freedom numbering with the original. Only we replace the original fields Fi, and Gi with

$$\tilde{\Gamma}_i \equiv \frac{\partial A}{\partial \nabla u_i} \qquad \tilde{F}_i \equiv \frac{\partial A}{\partial u_i} \qquad \text{and} \qquad \tilde{G}_i \equiv \frac{\partial B}{\partial u_i} \tag{46}$$

Assembling the right-hand-side vector eL i with this definition yields exactly Eq. (28), c.f. Eq. (20). An extra convenience in is that we can rely on the built-in symbolic differentiation tools to compute the derivatives ∂A/∂ui etc. In order to try out a new objective for the optimization problem, the user essentially only needs to change the text expressions defining the quantities A and B. After solving the adjoint problem Eq. (23) to eliminate ∂Ui for i = 1, 2, 3 in Eq. (22b) we can evaluate the sensitivity

$$\frac{d}{d\gamma}\left[\Phi(\mathbf{U},\gamma)\right] = \frac{\partial \Phi}{\partial \gamma} + \sum_{j=1}^{3} \left(\frac{\partial \mathbf{L}_j}{\partial \mathbf{U}_i}\right)^T \tilde{\mathbf{U}}_j - \left(\frac{\partial \mathbf{M}_j}{\partial \gamma}\right)^T \tilde{\Lambda}_j$$

$$= \tilde{\mathbf{L}}_4 - \sum_{j=1}^{3} \mathbf{K}_{j4}^T \tilde{\mathbf{U}}_j - \mathbf{N}_{j4}^T \tilde{\Lambda}_j \tag{47}$$

where Ki4 = −∂Li/∂ , Ni,4 = −∂Mi/∂ , and eL 4 = ∂/∂ in accordance with U4 ≡ γ. Since the fourth variable γ is treated on equal footing with the other three variables, all expressions required to compute the matrices Ki,4 and Ni,4 come out of the standard linearization of the problem. This is yet another advantage of including γ as an extra dependent variable. When dealing with a problem with a volume constraint as in Eq. (15b), it is necessary to compute the derivative of the constraint with respect to ,

$$\frac{\partial}{\partial \gamma}\left[\frac{1}{|\Omega|}\int_{\Omega} \gamma(\mathbf{r})\, d\mathbf{r} - \beta\right] = \frac{1}{|\Omega|}\int_{\Omega} \varphi_{n,4}(\mathbf{r})\, d\mathbf{r} \tag{48}$$

The optimization problem is stated as a minimization of the horizontal fluid velocity at the point r∗ at the center of the channel, i.e., the design objective is

$$\Phi = v_1(\mathbf{r}^*) \tag{49}$$

In terms of the general objective Eq. (11) this is obtained with

$$A \equiv v_1(r)\delta(r - r*) \tag{50}$$

and

$$B \equiv 0. \tag{51}$$

There is no explicit need for a volume constraint because neither of the extreme solutions of completely filled or empty can be optimal. When the design domain is completely filled with magnetic field we expect a flat flow profile with magnitude below

$$v0 < p/(5\ell\alpha\max). \tag{52}$$

In the other extreme case when the channel is completely devoid of magnetic field the solution is simply a parabolic Poiseuille profile with maximum

$$v_0 = \frac{\eta}{8l^2}\frac{\Delta p}{L} \tag{53}$$

However, a structure that reverses the flow such that $v_1(r*)$ becomes negative will be superior to both these extreme cases in the sense of minimizing $\Phi_0 = \frac{96}{9}\left(4 + \frac{L}{l}\right)\eta v_{\max}^2$.

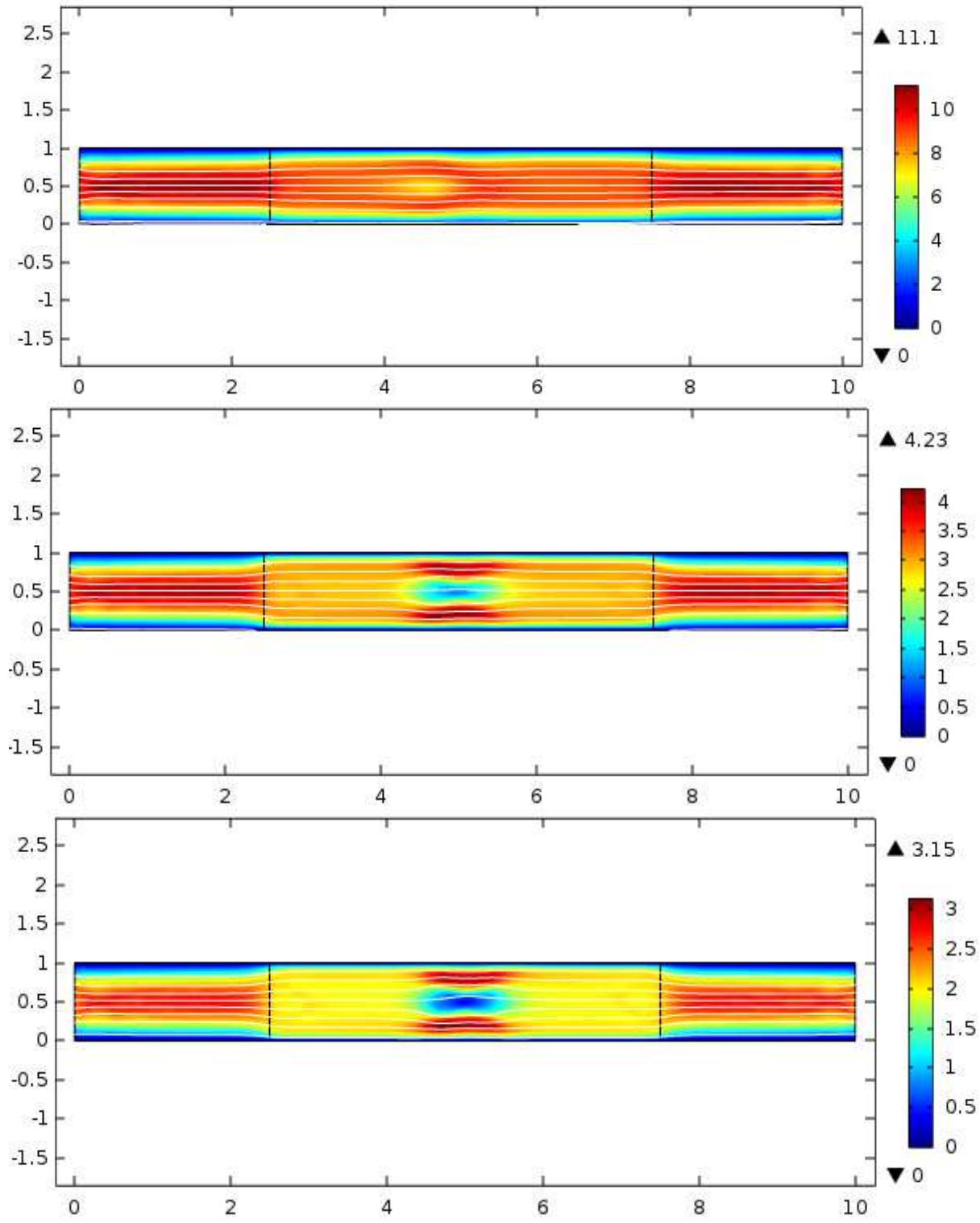
▲ 11.1
10
8
6
4
2
0
▼ 0
▲ 4.23
4
3.5
3
2.5
2
1.5
1
0.5
0
▼ 0
▲ 3.15
3
2.5
2
1.5
1
0.5
0
▼ 0

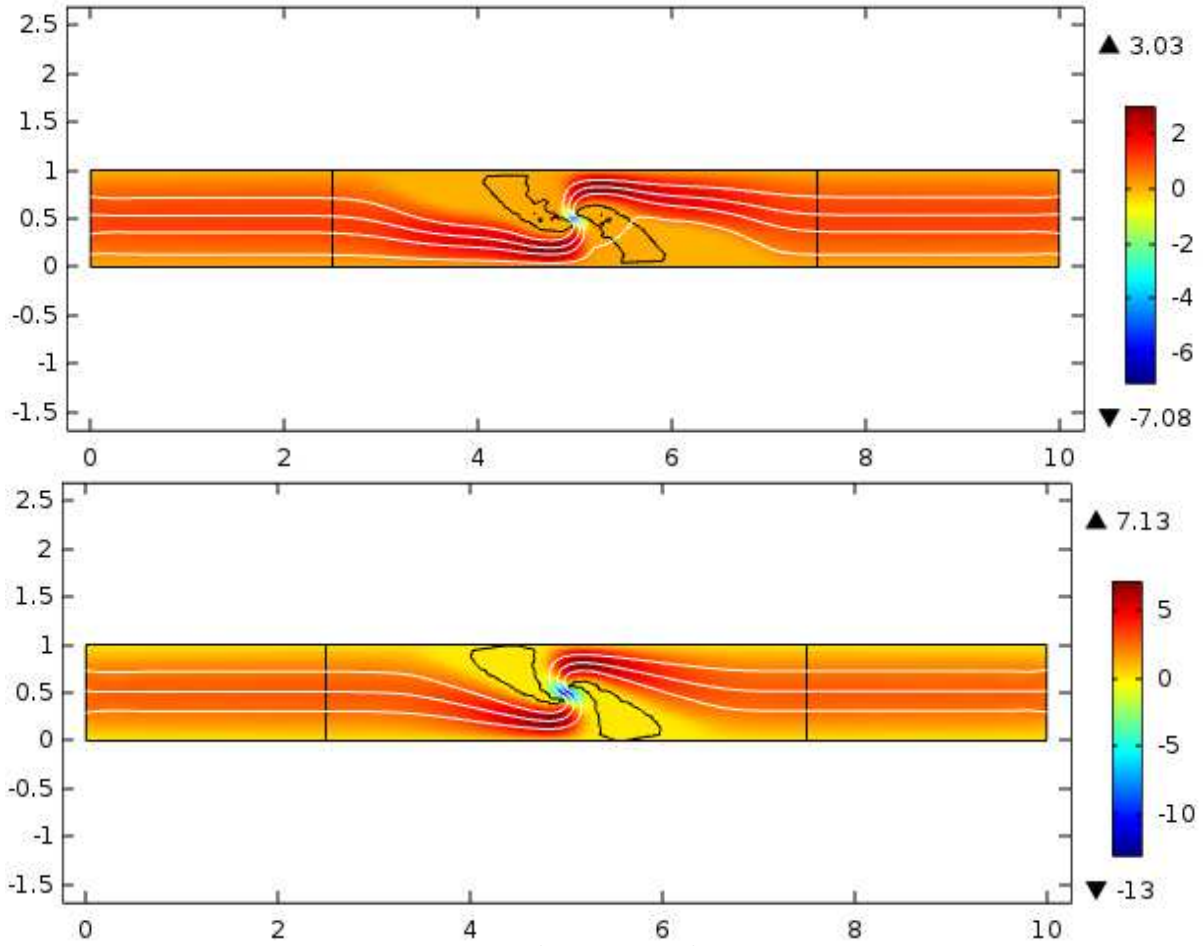

Fig.2. Velocity field in process of optimization

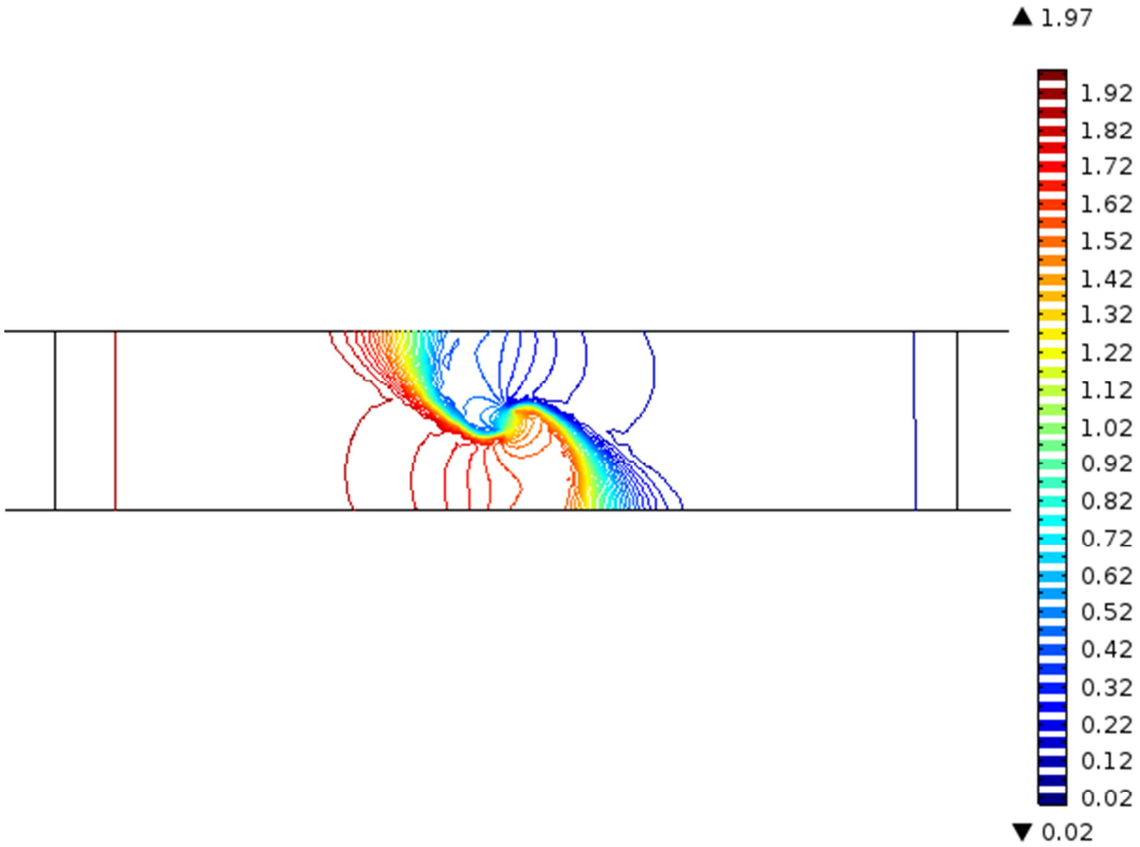

Fig.3. Optimized structures pressure distribution at p_{in} = 2

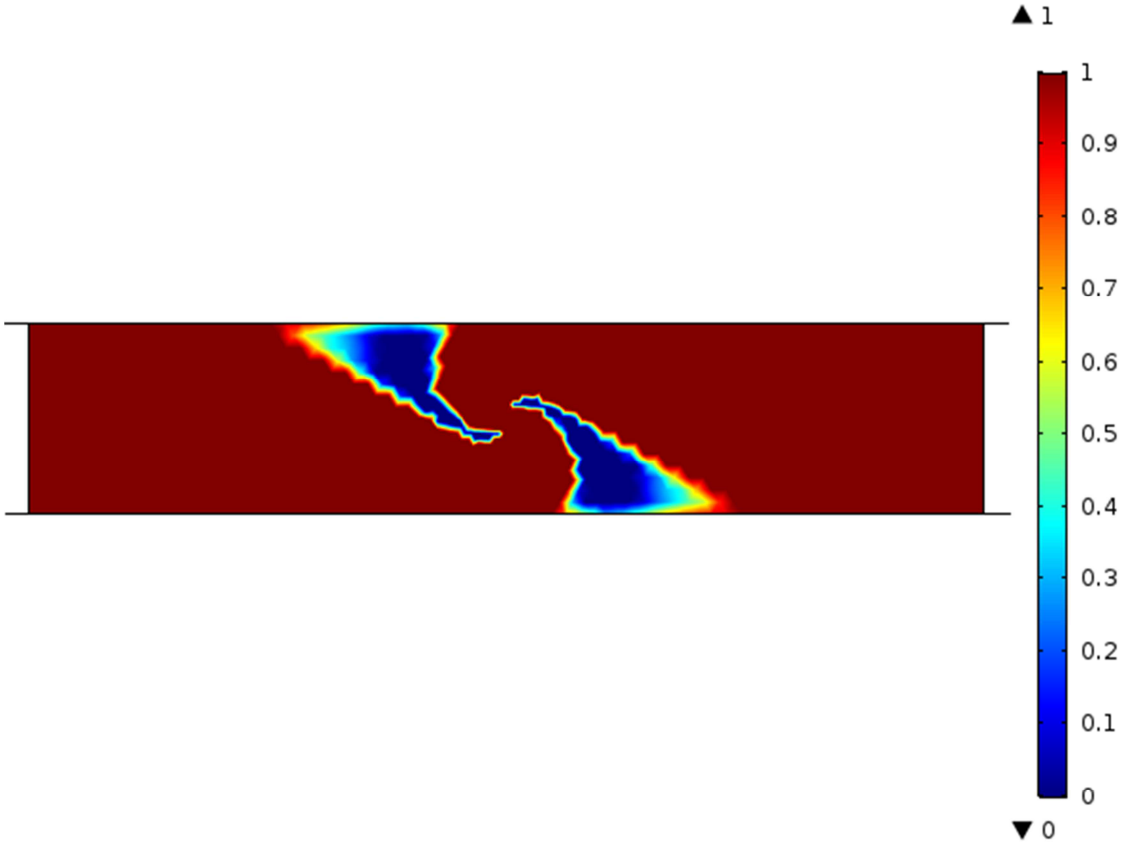

Fig.4. Optimized dimensionless external magnetic distribution at p_{in} = 2

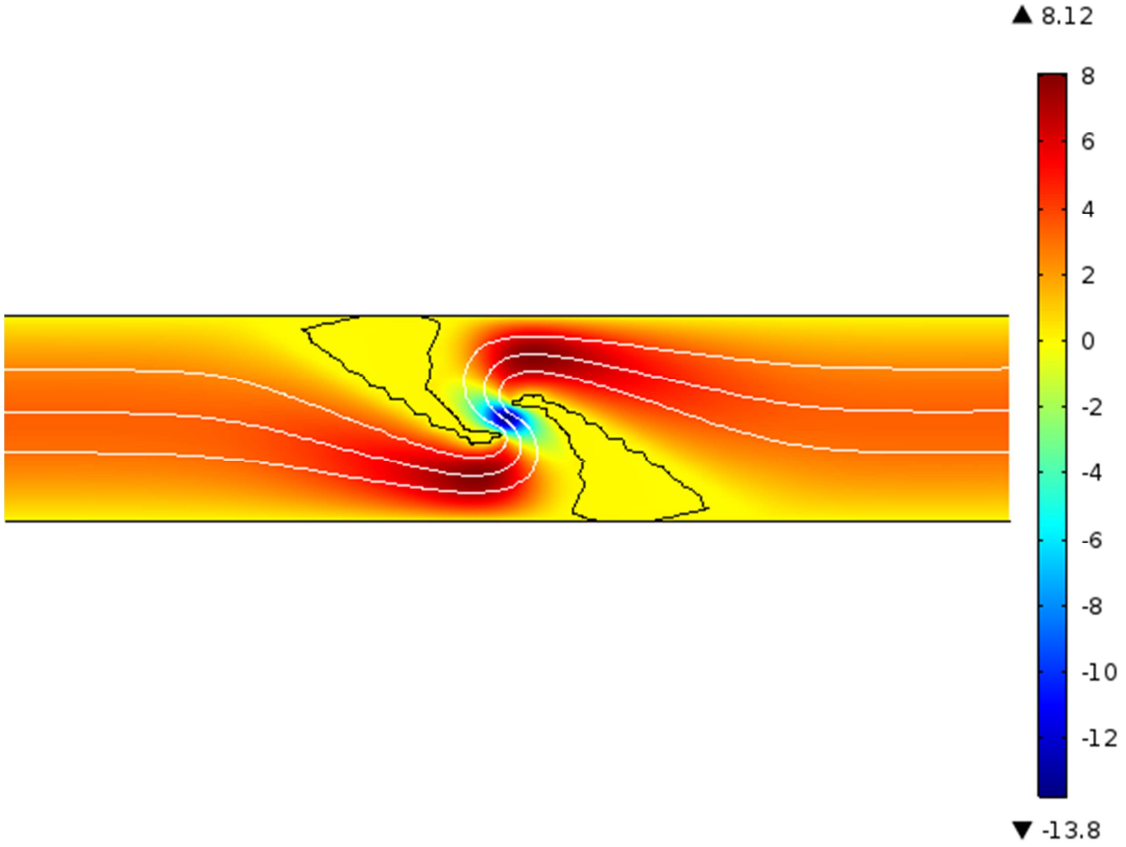

Fig.5. Optimized velocity distribution at p_{in} = 2

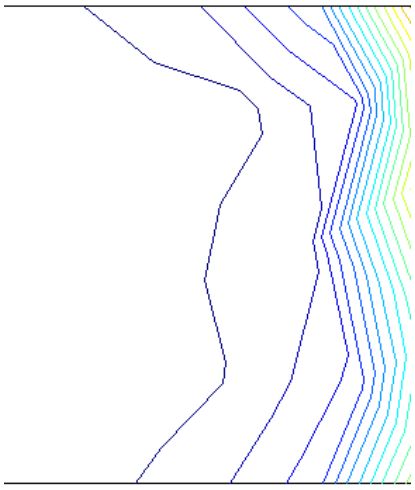

Fig.6. Optimized concentration distribution at p_{in} = 2

A question that naturally arises in this type of problems concerns uniqueness of the solution. In this case, there is at least one more solution that gives exactly the same result; because the channel has no upside or downside, a solution mirrored around the axis y=0.5 mm would give exactly the same flow. Figure 3 contains a surface plot of the horizontal velocity component and a streamline plot of the velocity field resulting from the optimization process. In addition, the contour indicates the border between the open channel and filling material. The plots reveal how the flow turns around, with a negative horizontal velocity at the center of the channel. Note also that the x-velocity has a minimum of roughly14 mm/s at the design point. If you were to increase the streamline density in the above plot, some streamlines passing through the barriers would appear. This effect is due to a small amount of leakage, which can be reduced further by increasing the mesh resolution.

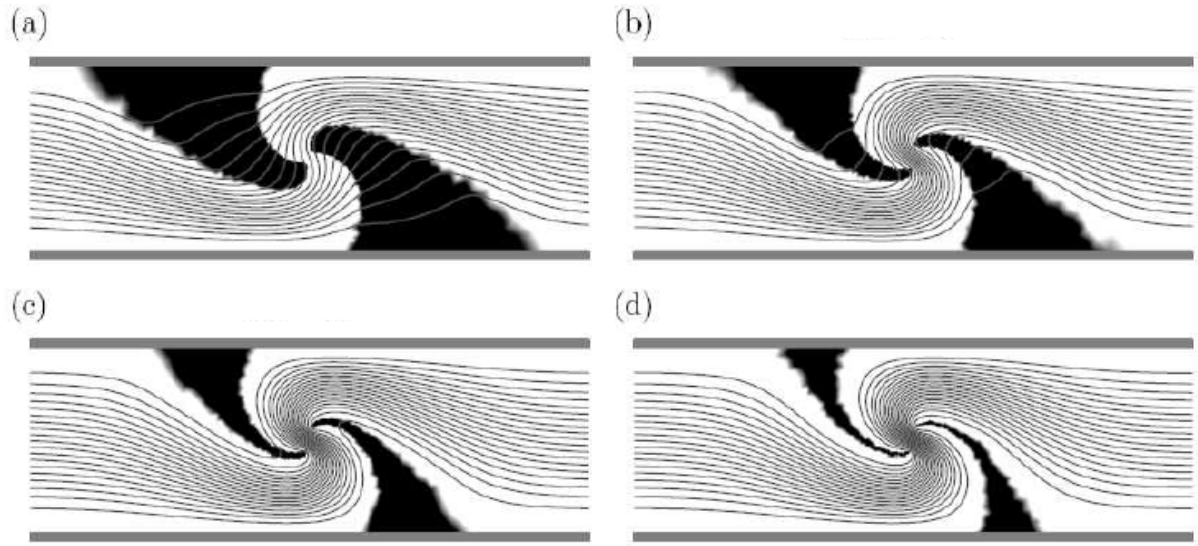

Fig.7. Optimized structures (black) and streamlines at 5% intervals for Stokes flow (Re = 0) at Hartmann numbers decreasing from 10−3 to 10−6. Only the central part of length 3ℓ of the design domain is shown. The structures consist of two barriers defining an S-shaped channel that reverses the flow at the central point r————————————. As the Hartmann number is decreased, the optimized structures become thinner and less permeable

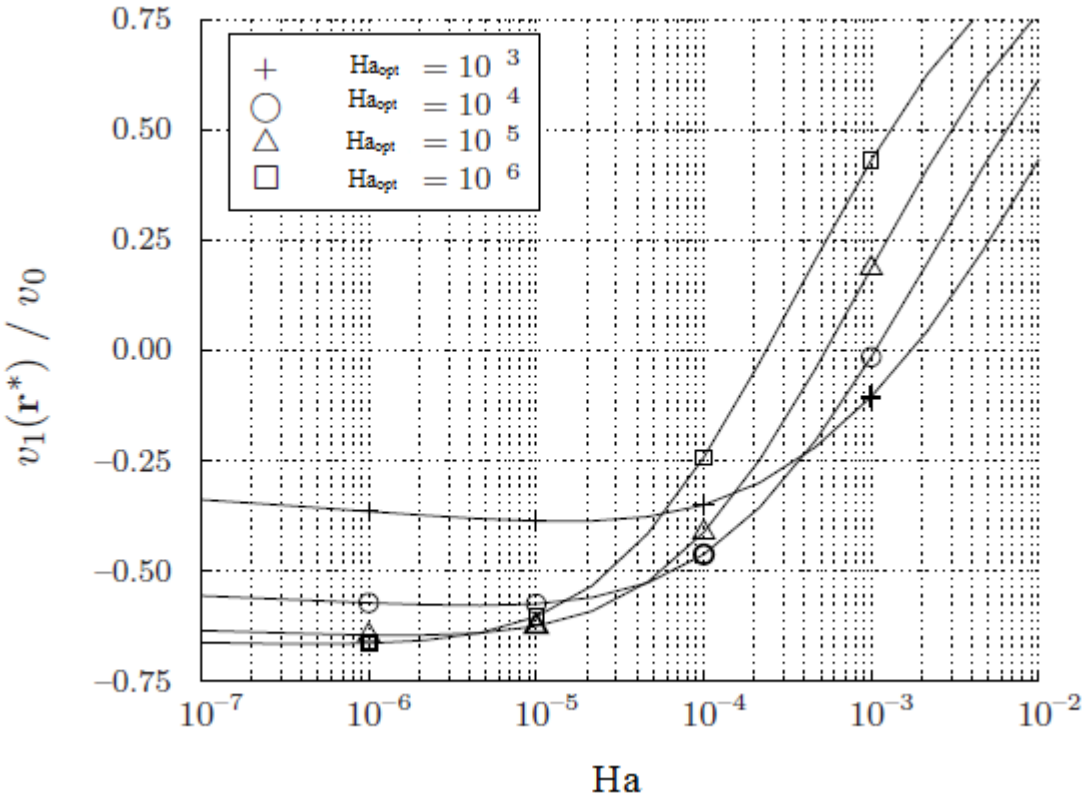

Fig.8. Comparing the performance of the structures from Fig. 2 optimized at Ha_{opt} for different values of Da. The objective v1(r————————————) is normalized with the velocity in an empty channel, v0, c.f. Eq. (33)

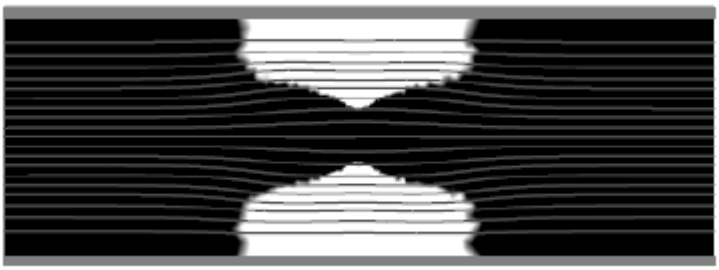

Fig.9. Optimized structure (black) and streamlines for Stokes flow at Da = 10−2; only the central part of length 3ℓ. The design domain is completely filled with magnetic field, except immediately above and below r———————————————— where two empty regions emerge. These voids divert the flow away from r————————————————, resulting in a low velocity v1(r————————————————) = 0.1v0

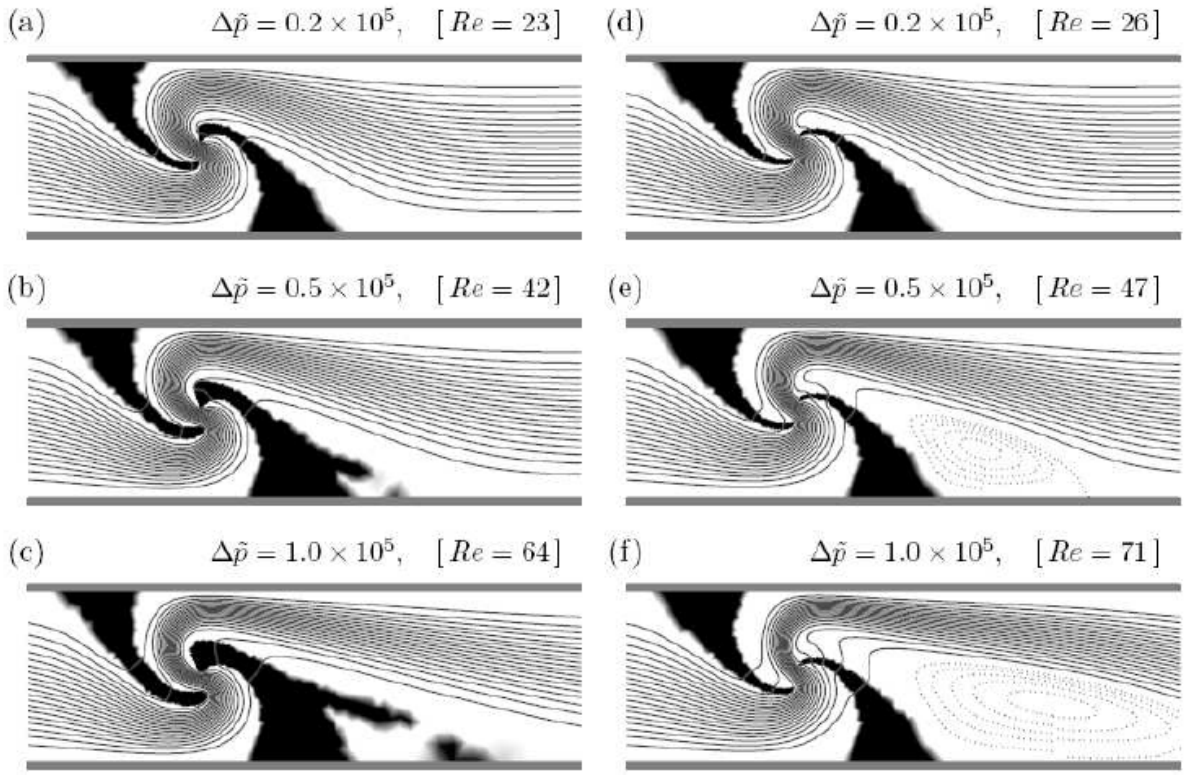

Fig.10. Optimized structures (black) and streamlines for Navier–Stokes flow; only a part of length 3.25ℓ near the center of the channel is shown. Panel (a)-(c) to the left show the optimized structures for different values of the control parameter ˜p = p ρℓ2/η2. For comparision the flow field when the optimized structure from Fig. 2(c) is frozen and exposed to the elevated pressure drops is shown in panel (d)-(f) to the right. The Reynolds number is defined as Re = ρ ℓ vmax/η where vmax is the maximal velocity measured at the inlet; note that for a particular value of ˜p, the Reynolds number is not fixed but differs slightly between left and right column

We first consider the Stokes flow limit of small p where the inertial term becomes neglible. The problem is then linear and the solution is characterized by a single dimensionless parameter, namely the Hartmann number Da, Eq. (6). We have solved the topology optimization problem for different values of Da. The initial condition for the magnetic field distribution was $\gamma(0) = 1$, and the parameter q determining the shape of $\alpha(\gamma)$ in Eq. (4) was set to q = 0.1. Anticipating that the structural details close to $r*$ should be more important than those further away we chose a non-uniform finite element mesh with increased resolution around $r*$. Fig. 2 shows the optimal structures obtained for Da = 10−3, 10−4, 10−5, and 10−6. They all consist of two barriers defining an S-shaped channel that guides the fluid in the reverse direction of the applied pressure drop. At Da = 10−3 the two barriers are rather thick but leaky with almost all the streamlines penetrating them; as the Hartmann number is decreased the optimal structures become thinner and less penetrable. This result can be interpreted as a trade-off between having either thick barriers or wide channels. Thick barriers are necessary to force the fluid into the S-turn, while at the same time the open channel should be as wide as possible in order to minimize the hydraulic resistance and maximize the fluid flow at the prescribed pressure drop. Notice that if we had chosen to prescribe the flow rate through the device rather than the pressure drop, then the optimal solution would have been somewhat different. When the flow rate is prescribed, it pays to make the gap between the barriers very small and the barriers very thick in order to force the fixed amount of fluid flow through the narrow contraction. The optimal structure is therefore one with a very large hydraulic

resistance. In Ref. [8] this problem was circumvented by adding a constraint on the maximal power dissipation allowed at the given flow rate. In order to validate the optimality of the structures computed by the topology optimization we do as follows: For each of the optimized structures from Fig. 2 we freeze the magnetic field distribution and solve the flow problem for a range of Hartmann numbers. The resulting family of curves for v1(r∗) vs. Da is shown in Fig. 3 where it is seen that each of the four structures from Fig. 2 do indeed perform better in minimizing v1(r∗) than the others at the value of Da for which they are optimized. For Da . 10−5 the optimal value of v1(r∗) tends to saturate because the thin barriers are then almost completely impermeable and the open channel cannot get much wider. In this limit the thickness of the optimized barrier structures approach the mesh resolution as seen in Fig. 2(d). When the optimal barrier thickness gets below the mesh size we have observed the appearance of artificial local optima for the barrier structure. The problem is that the thin barriers cannot continuously deform into another position without going through an intermediate structure with barriers that are thicker by at least one mesh element. Depending on the initial condition, the optimization algorithm can therefore end up with a sub-optimal structure. We have tried to work around this problem by decreasing the value of q in order to smear out the solid/void interfaces and thus reduce the cost of going through the intermediate structure. This did not work out well; the reason may be that the smearing property of a convex α(γ) was derived for the objective of minimizing the power dissipation subject to a volume constraint. In the present example we are dealing with a different objective and have no volume constraint. However, when the barrier structures are resolved with at least a few elements across them the artificial local optima tend to be insignificant. Thus the problem can be avoided by choosing a sufficiently fine mesh, or by adaptively refining the mesh at the solid/void interfaces. Returning to Fig. 3 we notice that as Da increases all the structures perform poorly in minimizing v1(r∗), as they all approach v0. Extrapolating this trend one might suspect that the S-turn topology will cease to be optimal somewhere above Da = 10−3 simply because the magnetic field becomes too permeable to make reversal of the flow direction possible. We have tested this hypothesis by performing an optimization at Da = 10−2, resulting in the structure shown in Fig. 4 where the value of the objective is v1(r∗) = 0.1v0. It is seen to display a different topology from those of Fig. 2, with the design domain is a symmetric structure blocking the flow like that in Fig. 4. However at a certain point in the iterations an asymmetry in the horizontal plane is excited and the structure quickly changes to the two-barrier S-geometry. Whether the optimization converge to an S- or an inverted S-turn depends how the asymmetry is excited from numerical noise or irregularity in the finite element mesh; in fact the structure in Fig. 2(b) originally came out as an inverted S but was mirrored by hand before plotting it to facilitate comparison with the three other structures.

CONCLUSION

Based on the work of Borrvall and Petersson we have extended the topology optimization of fluid networks to cover the full incompressible Navier–Stokes equations in steady-state. Our implementation of the method is based on the commercial finite element package , which reduces the programming effort required to a minimum. 17 Formulating the problem in terms of a general integral-type objective function and expressing the governing equations in divergence form makes the implementation very compact and transparent. Moreover the code for performing the sensitivity analysis should remain almost the same for any problem expressed in this way, whereas that required for describing the physical problem of course changes. Topology optimization of multi-field problems can therefore be dealt with almost as easy as a single realization of the underlying physical problem. We would like to mention that our methodology is not as such restricted to the (large) class of physical problems that can be expressed in divergence form. This does in fact not invalidate the sensitivity analysis worked out, since this analysis only relies on the basic structure of the discretized nonlinear problem and the availability of the Jacobian matrix. It is therefore possible to apply our methodology to even larger classes of physical problems than the ones comprised by the divergence form. Our implementation of topology optimization has been tested on two fluidics examples in 2D, both illustrating the influence of different quantities and conditions on the efficiency of the optimization method. The first example, a channel with reversed flow, illustrates the influence of the Reynolds number Re and the Hartmann number Da on the solutions. We have shown that the choice of Ha has a strong impact on the solution when the structure contains barriers to deflect the fluid stream. The second example, minimization of the power dissipation in a four-terminal device, reveals the problems of determining the global minimum when two strong minima are competing. This problem is highly non-convex, and we have shown that the solution depends on the initial condition. For an initial homogeneous magnetic field distribution, the friction dominates and the solution does not come out as the global optimum in all cases. Using an empty channel as the initial state, inertia plays a role from the beginning, and better results can be obtained. However, this initial condition in fact violates the volume constraint, and the part of the optimization routine correcting this depends on a penalty factor. Unfortunately, the particular value chosen for this factor strongly influences the results. Increasing the Hartmann number makes the problem more convex, but continuation from large to small Ha, i.e., from high to low magnetic field strength of the magnetic field, does not generally end up in the global optimum. In conclusion, we have shown that our implementation of topology optimization is a useful tool for designing fluidic devices.

REFERENCES

[1] MY Abdollahzadeh Jamalabadi, *J Media*, **2015**, 18(9) ,843-860.
[2] MY Abdollahzadeh Jamalabadi; JH Park, *Therm Sci*, **2014**, 94-94
[3] MY Abdollahzadeh Jamalabadi, *Int J Opt Appl*, **2015**, 5 (5) , 161-167
[4] MY Abdollahzadeh Jamalabadi, *Chem Eng Res Des*, **2015**, 102 , 407-415
[5] MY Abdollahzadeh Jamalabadi ; JH Park, *World App Sci Journal* , **2014**, (4)32 , 672-677
[6] MY Abdollahzadeh Jamalabadi; JH Park ; CY Lee, *entropy*, **2015**, 17 (2), 866-881
[7] A Shahidian; M Ghassemi; S Khorasanizade; M Abdollahzade; G Ahmadi, *IEEE Trans Magn*, **2009**, 45 (6)2667-2670
[8] MY Abdollahzadeh Jamalabadi, *J. Marine Sci & App*, **2014**, 13 (3) 281-290
[9] MY Abdollahzadeh Jamalabadi ; JH Park, *Int J. Sci Basic App Res Sci* 1 , **2014**, 421-427
[10] MY Abdollahzadeh Jamalabadi ; JH Park, *Open J. Fluid Dyn*, **2014**, 23 (4) 125-132
[11] MY Abdollahzadeh Jamalabadi;JH Park;MM Rashidi ;JM Chen, *J. Hydrod Ser*. B, **2016**
[12] MY Abdollahzadeh Jamalabadi, *Front Heat Mass Trans*, **2015**, 6,013007
[13] M.Y. Abdollahzadeh Jamalabadi, J. *Fuel Cell Sci. Technol*, **2013**, 10(5) , 1039
[14] MY Abdollahzadeh Jamalabadi;JH Park; CY Lee, *Therm Sci*, **2014**, 124-124
[15] M Jamalabadi; P Hooshmand; B Khezri ; A Radmanesh, *Ind J sci Res* 2 , **2014**, 74-81
[16] MY Abdollahzadeh Jamalabadi, *Mul Model Mat Struc* , **2016**
[17] M.Y. Abdollahzadeh Jamalabadi, J.H.Park,C.Y. Lee, *International Journal of Applied Environmental Sciences*, **2014**, 9 (4) 1769-1781
[18] MY Abdollahzadeh Jamalabadi, *World App. Sci. J.* **2014**, 32 (4) 667-671
[19] MY Abdollahzadeh Jamalabadi, *Mid-East J. Sci Res* **2014**, 22 (4)561-574
[20] MY Abdollahzadeh Jamalabadi, *Mat . Perf. Char*, **2015** 20140062
[21] MS Shadloo;R Poultangari; MY Abdollahzadeh Jamalabadi, MM Rashidi, *Energy Conversion and Management*, **2015**,96 , 418-429
[22] MY Abdollahzadeh Jamalabadi; M Ghasemi; MH Hamedi, *Int J Numer Meth Heat Fluid Flow*, **2013**, 23 (4) 649-661
[23] MY Abdollahzadeh Jamalabadi, *Int J Ener Mat Chem Pro*,**2016** 15, DOI:10.1615/IntJEnergeticMagnetic fieldsChemProp.2015014428
[24] MY Abdollahzadeh Jamalabadi, *Noise and Vibration Worldwide*,**2014**, 45 (8) 21-27
[25] MY Abdollahzadeh Jamalabadi, *J. King Saud Univ Eng Sci*,**2014**, 26 (2) 159-167
[26] MY Abdollahzadeh Jamalabadi ; M Ghasemi ;MH Hamedi, *Proc Inst Mech Eng, Part C, J. Mech Eng Sci*,**2012** ,(226) 1302-1308
[27] M.Y. Abdollahzadeh Jamalabadi, *Int J Ener Eng*, **2015**, 5(1) 1-8
[28] M.Y. Abdollahzadeh Jamalabadi, *Int J Mult Res Dev*,**2014**, (1) 5 ,1-4
[29] MY Abdollahzadeh Jamalabadi,S Dousti, *J of Chem and Pharm Res*, **2015** (7) 12:206-218
[30] MY Abdollahzadeh Jamalabadi,M Ebrahimi,G Homayoun,P Hooshmand, *J of Chem and Pharm Res*, **2015** (7) 12 : 788-799
[31] MY Abdollahzadeh Jamalabadi, *Mat Per and Char* **2015**(4) 1 :1-28
[32] MY Abdollahzadeh Jamalabadi, *J of Niger Math Soc*, **2016**
[33] MY Abdollahzadeh Jamalabadi, *J of Chem and Pharm Res*, **2016**, (8) 2 : 448-469
[34] MY Abdollahzadeh Jamalabadi and Ovisi, M, *J of Chem and Pharm Res*, **2016**, (8) 1 : 712-728
[35] MY Abdollahzadeh Jamalabadi and Keikha, A., *J of Chem and Pharm Res*, **2016**, (8) 2: 428-442
[36] P Hooshmand; MY Abdollahzadeh Jamalabadi; H K Balotaki; *Int Journal of Pharm Res and Allied Sci*, **2016** (5) 2 : 293-304
[37] MY Abdollahzadeh Jamalabadiand Keikha, A., *Ent and App Sci Let*, **2016**, 3, 2:
[38] R Patakfalvi;Dekany, *Colloid* Polym Sci,**2010**, 280, 461–470.
[39] MY Abdollahzadeh Jamalabadi, Dousti, M; *Int Jof Res and Rev in App Sci*, **2016**26,1 : 1-19
[40] MY Abdollahzadeh Jamalabadi, Dousti,S; *Int Jof Res and Rev in App Sci*, **2015**25,3 :55-63
[41] MY Abdollahzadeh Jamalabadi, *Int J of Eng and App Sci* **2015** (7) 51-21
[42] MY Abdollahzadeh Jamalabadi, Oveisi, M*; J of App Math and Phys*, **2016**4 : 398-411
[42] MY Abdollahzadeh Jamalabadi, *EFC 2013* ,**2013** 395-396
[43] PV Asharani; YL Wu; Z Gong; S Valiyaveettil, *Nanotechnology* ,**2008**, 19, 1–8.
[44] K Bilberg; MB Hovgaard; F Besenbacher; E Baatrup , *J Toxicology* ,**2012**, 293784,1-9.
[45] K Bilberg, H Malte, T Wang, E Baatrup , *Aquatic Toxicology* ,**2012**, 96,159-165.
[46] MY Abdollahzadeh *Jamalabadi*, **2015**(5) 2 :118-124
[47] P Jegadeeswaran; R Shivaraj; R Venckatesh ,*Digest J Nanomagnetic fields Biostructures* ,**2012**,7, 991 – 998.
[48] QA Pankhurst; NK T Thanh; SK Jones; and J Dobson, *J. Phys. D: Appl. Phys*., **2003**, 36, 13, 167–181.
[49] L Johannsen; J O Blanchette, *Adv. Drug Deliv*, **2004**, 56, 1649–1659.

[50] M E Davis; Z Chen; D M Shin, *Nat. Rev. Drug. Discov*, **2008**, 7, 771–782.
[51] M Arruebo; R Fernandez-Pacheco; M R Ibarra; J Santamaria, *Nano Today*, **2007**, 2, 22-32.
[52] C Alexiou; R Jurgons; C Seliger; O Brunke; H Iro; S Odenbach, ,*Anticancer Res*,**2007**, 27, 4A, 2019–2022
[53] S I Takeda; F Mishima; S Fujimoto; Y Izumi; S Nishijima, *J Magn. Magn. Mater*, **2006**,311, 367-371.
[54] K B Yesin; K lmers; B J Nelson; *Int. J. Robot. Res*, **2006**, 25, 527-536
[55] J J Abbott; O Ergeneman; M P Kummer; A M Hirt; B J Nelson, *IEEE Trans. Robot*, **2007**, 23, 1247-1252
[56] C Alexiou; D Diehl; P Henninger; H Iro; R Rockelein; W Schmidt; H Weber, *IEEE Trans. Appl. Supercond*, **2006**, 16, 1527–1530
[57] X Han; Q Cao; and L Li, *IEEE Trans. Appl. Supercond*, **2012**, 22, 3, 4401404– 4401404
[58] J-B Mathieu; S Martel, *Biomed Microdevices*,**2007**,9, 801–808
[59] S Martel; O Felfoul; J-B Mathieu; A Chanu; S Tamaz; M Mohammadi; M Mankiewicz; N Tabatabaei, *Int. J. Rob. Res*, **2009**, 28, 9, 1169–1182
[60] H Choi; J Choi; G Jang; J Park; S Park, *Smart Mater. Struct*, **2009**, 18, 5, 055007
[61] S Jeon; G Jang; H Choi; S Park, *IEEE Trans. Magn*, **2010**,46, 6, 1943–1946
[62] H Choi; K Cha; J Choi; S Jeong; S Jeon; G Jang; J Park; S Park, *Sens. Actua. A: Phys*, **2010**, 163, 1, 410–417
[63] S Bita; MY Abdollahzadeh Jamalabadi, MY; M Mesbah, *J. Chem. Pharm. Res*., **2015**, 7(11):91-98
[64] MY Abdollahzadeh Jamalabadi; Kim , SW; Lee , CY ; Park, JH, *Adv in Mech Eng*, **2016** (8) 4 :1-10
[65] MY Abdollahzadeh Jamalabadi;Hooshmand, P ; Bagheri, N, KhakRah, H;Dousti, M; *entropy*, **2016** (18) 4 :147-161
[66] MY Abdollahzadeh Jamalabadi, *Int J of Ener Mat and Chem Prop*, **2015** (15) 1 : 65-88